JOURNAL OF GEOPHYSICAL RESEARCH, VOL. 115, B06206, doi:10.1029/2009JB006985, 2010

Unsteady high-pressure flow experiments with applications to explosive volcanic eruptions

M. M. Orescanin,[1] J. M. Austin,[2] and S. W. Kieffer[1]

Received 17 September 2009; revised 23 December 2009; accepted 14 January 2010; published 23 June 2010.

[1] Motivated by the hypothesis that volcanic blasts can have supersonic regions, we investigate the role of unsteady flow in jets from a high-pressure finite reservoir. We examine the processes for formation of far-field features, such as Mach disk shocks, by using a shock tube facility and numerical experiments to investigate phenomena to previously unobtained pressure ratios of 250:1. The Mach disk shock initially forms at the edges of the vent and moves toward the centerline. The shock is established within a few vent diameters and propagates downstream toward the equilibrium location as the jet develops. The start-up process is characterized by two different timescales: the duration of supersonic flow at the nozzle exit and the formation time of the Mach disk shock. The termination process also is characterized by two different timescales: the travel time required for the Mach disk shock to reach its equilibrium position and the time at which the Mach disk shock begins significantly to collapse away from its equilibrium position. The critical comparisons for the formation of steady state supersonic regions are between the two start-up timescales and the termination timescales. We conclude that for typical vulcanian eruptions and the Mount St. Helens directed blast, the Mach disk shock could have formed near the vent, and that there was time for it to propagate a distance comparable to its equilibrium location. These experiments provide a framework for analysis of short-lived volcanic eruptions and data for benchmarking simulations of jet structures in explosive volcanic blasts.

Citation: Orescanin, M. M., J. M. Austin, and S. W. Kieffer (2010), Unsteady high-pressure flow experiments with applications to explosive volcanic eruptions, *J. Geophys. Res.*, *115*, B06206, doi:10.1029/2009JB006985.

1. Introduction

[2] Explosive volcanic events ranging in size from short hydrothermal and vulcanian eruptions to longer Plinian eruptions result from the discharge of a pressurized reservoir into the atmosphere. Because the reservoir pressure is significantly higher than atmospheric pressure, the flow field of volcanic jets is complex, including supersonic and subsonic zones, internal standing and traveling waves, a complex shear layer, and interaction with boundaries and obstacles. The volume of material available for an eruption ranges from a fraction of a cubic kilometer (e.g., hydrothermal and vulcanian eruptions), to several hundred cubic kilometers and, in rare events, to over 1000 cubic kilometers. Direct measurement of the flow field of such eruptions is precluded, and scaled experiments and numerical simulations are essential for understanding the governing dynamics. The objective of our work is to provide such experiments and numerical simulations for relatively short eruptions where the finite size of the reservoir plays a significant role in the eruption dynamics.

[3] Eruption duration is dependent on the geometry and volume of the magma reservoir. *Melnick and Sparks* [2002] defined two end-member cases of magmatic eruptions: an "equilibrium case" where diffusion of volatiles in the magma into pores is so fast that the gas available for expansion at any time is a function of pressure alone; and "the no mass transfer case" in which the only gas available to drive the eruption is that which has been exsolved prior to the eruption. In this latter case, diffusion of volatiles is too small to supply more volatiles as the eruption proceeds. In an intermediate case, magma decompression may follow a no mass transfer history, but mixed hydrothermal material may follow an equilibrium path. *Clarke et al.* [2002a] review these cases in the context of formulating initial conditions for eruption models. Our investigations apply to the latter and intermediate cases and, therefore, are limited in application to smaller eruptions (e.g., a few cubic kilometers) because we do not consider the role of ongoing volatile production by decompression, and we do not consider the possible effect of resupply rate from depths in prolonging the duration. In addition, we consider only the duration of individual eruptive events, not prolonged eruption cycles. Specifically, we compare our results to the

[1]Department of Geology, University of Illinois at Urbana-Champaign, Urbana, Illinois, USA.
[2]Department of Aerospace Engineering, University of Illinois at Urbana-Champaign, Urbana, Illinois, USA.

0148-0227/10/2009JB006985

May 18, 1980 Mount St. Helens directed blast and to typical vulcanian eruptions, such as Soufrière Hills, Montserrat; Asama and Sakurajima, Japan; Aerinal, Costa Rica; and Ngauruhoe, New Zealand.

[4] The Mount St. Helens directed blast was likely an intermediate case because magmatic volatiles were present, however hydrothermal fluids were also present to augment the magmatic gases. The existence of a finite reservoir at Mount St. Helens was noted in previous studies and the duration of the directed blast at the vent was calculated by estimating the round-trip travel time for an expansion wave in a previously vesiculated reservoir [*Kieffer*, 1982]. This analysis yielded the duration of the blast at the vent as approximately 20 seconds. Because rarefaction waves broaden in time and with distance [*Liepmann and Roshko*, 2001], it was assumed that the steady state approximation could be used for the far field, but this result was not quantified. When we discuss Mount St. Helens, we use a volume of 0.1 km^3 [*Brodsky et al.*, 1999]. We use an average pressure ratio of 150:1, corresponding to initial conditions proposed by *Kieffer* [1981], and we discuss the sensitivity to other pressure ratios. Reservoir dimensions at Mount St. Helens are estimated to be 850 m in the east–west direction, 100 m in the north–south direction, and an inferred depth of 1300 m to give a discharge volume of approximately 0.1 km^3 [*Donnadieu and Merle*, 2001].

[5] Although there are few measurements on specific vulcanian eruptions, it is generally known that typical volumes are of the order 5×10^7 m^3, and eruption durations range from a few to a few tens of seconds (e.g. Soufrière Hills, Montserrat; Asama and Sakurajima, Japan; Aerinal, Costa Rica; and Ngauruhoe, New Zealand). At Ngauruhoe, cannon-like explosions in February, 1975 were well documented [*Nairn*, 1976; *Narin and Self*, 1978], but reservoir dimensions and mass ejected were only loosely constrained. The minimum volume ejected was 3.4×10^6 m^3 over seven separate explosions, for an average of about 0.5×10^6 m^3 per eruption, and the duration of these events seems to be less than 10 seconds from the descriptions of *Narin and Self* [1978]. In August 1997, vulcanian explosions at Soufrière Hills, Montserrat were similar: explosions lasting 10–20 seconds each and ejecting about 3×10^5 m^3 in each burst [*Sparks et al.*, 2002]. Conduit overpressure estimates range from 100–250 bars. These overpressures should produce a supersonic flow field. Even though direct measurement within vulcanian eruption plumes have not been made, supersonic conditions have been inferred from the behavior of atmospheric shock waves and numerical models [*Clarke et al.*, 2002a, 2002b].

[6] If reservoir pressures exceed atmospheric pressure by a factor of about two, then supersonic jets are predicted to form in the discharging flow field. Depending on the pressure ratio, these jets have a complex structure. For pressure ratios between 2:1 and 5:1, the main features are intersecting oblique shocks and the flow exhibits "regular reflection". For pressure ratios above about 5:1 [*Irie et al.*, 2003], the crossed oblique shocks widen and transform into barrel and Mach disk shocks and the flow exhibits "Mach reflection", forming a jet structure called an "underexpanded jet" (Figure 1a). The pressure ratio between the magma reservoir and ambient conditions typically exceeds 5:1, therefore it is likely that similar dynamics exist in volcanic plumes. With a steady state assumption, the underexpanded jet model for a volcanic blast was first proposed by *Kieffer* [1981, 1982, 1984] for the Mount St. Helens directed blast. This model explained certain observable geologic features, specifically the direction of tree blowdown and size and shape of the direct blast zone. However, when a jet exhausts from a finite volume, the reservoir pressure decreases due to internally reflecting expansion waves and gas exiting the reservoir. We examine conditions under which the time dependent pressure may effect the geometry of the venting jet.

[7] If the discharge is from a large reservoir, then steady state flow approximations may be appropriate, whereas if the reservoir is small, then unsteady effects may dominate. "Large" and "small" are quantified further in section 4.2. Some of the more interesting features of the flow field, such as the Mach disk shock, are at large distances from the vent, e.g., at distances of the order ten times the vent diameter, therefore emphasizing the need to understand the effects of a finite reservoir on jet structure. The influence of the finite reservoir could be to terminate the discharge before the far-field flow features have been established. In 1980 when *Kieffer* [1981] analyzed the directed blast at Mount St. Helens, unsteady flow models were unavailable. A steady state flow model had to be assumed for calculations to explain the observed contrast of tree blowdown patterns in the direct and channelized blast zones of the directed blast (Figure 1b) [*Kieffer*, 1981, 1982]. In section 4 we show that, in fact, steady flow conditions were obtained in the blast.

[8] Unsteady flow has been previously shown by numerical experiments to affect supersonic jet structure [*Irie et al.*, 2003]. In this study, the reservoir-to-ambient pressure ratio was varied from three to fifteen by continuously increasing or decreasing the ambient back pressure while holding the reservoir pressure constant. The location of the Mach disk shock location increased above steady state distances for decreasing back pressure and decreased below steady state distances for increasing back pressure. The critical pressure for Mach to regular reflection transition has also been reported to be dependent on the flow history and a hysteresis loop was calculated [*Irie et al.*, 2003; *Welsh*, 1997; *Gribben et al.*, 2000].

[9] Outstanding questions in applying the underexpanded jet model to volcanic eruptions from a finite reservoir are: Does the flow history play a role in jet evolution? What is the jet structure and can it be predicted from steady state theory if the reservoir pressure history is known? What is the timescale for establishment of supersonic flow features and how does it compare to the reservoir discharge time? What are the conditions under which a Mach disk shock is established at its equilibrium position in the far field?

[10] In this paper, we examine the relationship between reservoir discharge times, or "blowdown times", and the establishment of features, such as the Mach disk shock, in the far field of supersonic jets in an attempt to answer the stated questions. We investigate here the relations between magmatic conditions, reservoir volume, and eruption duration for explosive eruptions through three-dimensional laboratory experiments supplemented by axially symmetric numerical simulations which we use qualitatively to aid and extrapolate our laboratory experiments. The methodology can be applied to evaluate the flow regimes and structure of

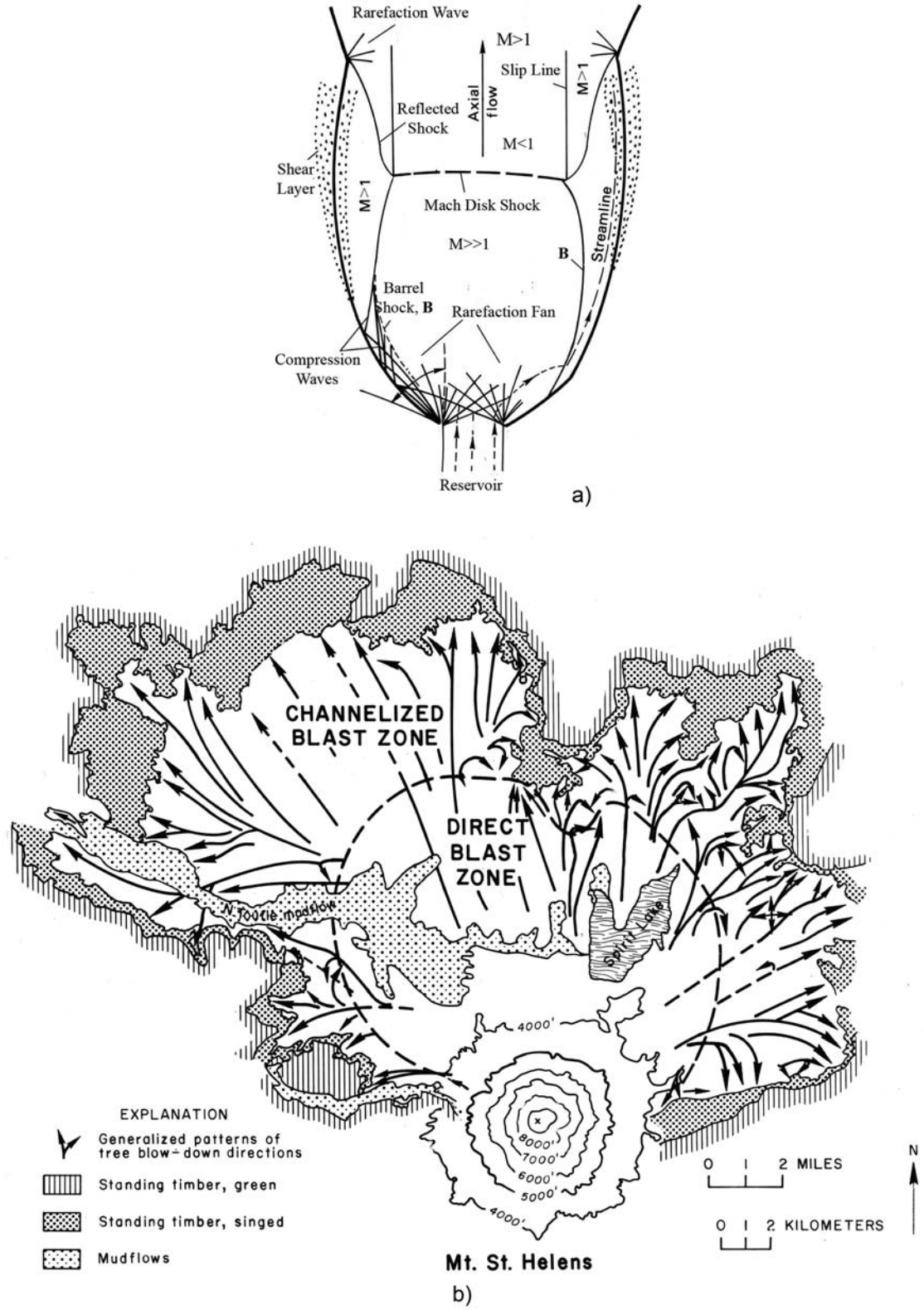

Figure 1. (a) Schematic of underexpanded jet flow structure showing supersonic (M > 1) and subsonic (M < 1) flow regions. (b) Schematic map of devastated area on the north flank of Mount St. Helens. Two distinct regions are: an inner direct blast zone, and an outer channelized blast zone. Images taken from *Kieffer* [1982].

Table 1. Experimental Text Conditions[a]

Pressure Ratios	Reservoir Gas Composition	γ	c_0 (m/s)	W (kg/mol)
250:1 to 15:1	Nitrogen	1.40	353	28
40:1 to 15:1	Helium	1.67	1002	4
250:1 to 100:1	Pseudogas	1.04	105	700

[a]Here γ is the isentropic exponent, c_0 is the speed of sound in the reservoir, and W is the molecular weight of the reservoir gas. Also shown are the conditions assumed for a pseudogas, based on *Kieffer* [1981].

eruptions from finite reservoirs of different vent area to reservoir volume ratios.

[11] Experimental investigations are performed over a range of initial pressure ratios up to 250:1. We describe results primarily for the initial conditions of the Mount St. Helens directed blast (pressure ratio of 150:1) as postulated by *Kieffer* [1981], but include sensitivity studies for pressure ratios from 100:1 to 250:1 to cover a typical range of similar eruptions, including vulcanian eruptions. We use helium, a good analogue for steam, and nitrogen as test gases venting into air.

[12] Precise timing of events makes it difficult to experimentally image the jet startup, which occurs over less than a millisecond, therefore we rely on numerical simulations to examine the early stages in jet formation. The numerical simulations were performed using the Amrita environment (J. J. Quirk, Amrita: A computational facility for CFD modeling, http://www.amrita-cfd.org/doc, 1998a; J. J. Quirk, Amr_sol: Design principles and practice, http://www.amrita-cfd.org/doc, 1998b), which incorporates adaptive mesh refinement and has been used extensively for compressible flows. We note that numerical simulations of volcanic plumes with supersonic cores near the vent cannot correctly capture the downstream subsonic conditions if the supersonic region is underresolved in the modeling.

[13] Multicomponent properties (e.g., gas plus entrained solids) are important [*Valentine and Wohletz*, 1989; *Valentine*, 1994, 1998; *Chojnicki et al.*, 2006; *Belousov et al.*, 2007], but techniques for visualizing flows of such mixtures are limited. There are additional complex physical processes (erosion, sedimentation, fragmentation of entrained materials), thermodynamic processes (heat transfer, evaporation, condensation) and geometric parameters of vent size and shape. By doing experiments with pure analog gases, a solid understanding of jet behavior can be described, to provide the foundation against which complications of actual eruptions can be compared. Safety and environmental considerations limit the use of fluids with isentropic exponent less than about 1.4 and we thus use thermodynamic scaling to apply our results to explosive volcanic eruptions. Using a typical rock/water mixture of 25:1, we describe this heavy fluid using a pseudogas model, with the isentropic exponent of 1.04 (calculations are available from *Kieffer* [1981]).

[14] The opening of a vent exposes the atmosphere to a high pressure reservoir. This can lead to the formation of a compression wave which can steepen into an atmospheric shock as in the case of Mount St. Helens [*Reed*, 1987], or to a strong atmospheric shock close to the vent [*Takayama and Saito*, 2004; *Saito et al.*, 1995]. The strength of the atmospheric shock depends on the properties of the erupting fluid [*Morrissey and Chouet*, 1997; *Chojnicki et al.*, 2006], and it may or may not contribute to the devastation. At Mount St. Helens, the compression wave was weak and did not contribute to the tree blowdown as evidenced in eyewitness photographs of the approaching blast [see also *Reed*, 1987] but it is well known that windows were knocked out by the atmospheric shock at distances over 150 km from the eruption during the Krakatoa eruption in 1833 [see also *Takayama and Saito*, 2004; *Saito et al.*, 1995]. The focus of the present study is the critical conditions for formation of shock structure internal to the jet and we do not address the atmospheric shock.

[15] The experimental setups for the laboratory and numerical experiments are described in section 2. Time-resolved images of jet structure during the discharge and pressure histories in the reservoir are presented in section 3. The effects of the unsteady inflow and decreasing reservoir pressure are examined in the context of existing steady state jet data in section 4. These results are discussed and applied to volcanic conditions in section 5.

2. Laboratory and Numerical Setup

[16] The experiments are designed to cover a range of conditions and parameters, particularly those estimated for vulcanian eruptions and the directed blast at Mount St. Helens. Reservoir to ambient pressure ratios varied with depth, and plausibly reached 250:1. We investigated pressure ratios up to 250:1, but present most of the laboratory results for a pressure of 40:1 because filming through the exhaust chamber windows used to attain 250:1 produced images of lesser quality; the features are the same as for the 40:1 when scaled to the higher pressure ratios. The test gases used in experiments include nitrogen, an analog to air, and helium, an analog to steam.

[17] To investigate the transient startup of the laboratory jets and complement experimental results, we carry out numerical simulations using the Amrita environment (Quirk, http://www.amrita-cfd.org/doc, 1998a; Quirk, http://www.amrita-cfd.org/doc, 1998b). The discharge of nitrogen jets from infinite and finite reservoirs with pressure ratios from 40:1 to 250:1 are investigated.

[18] The laboratory and numerical simulations are different from the Mount St. Helens directed blast conditions in two ways: thermodynamically and geometrically. First, the laboratory and numerical experiments are done with nitrogen and helium jets. These gases are thermodynamically different from the the directed blast fluid, particularly in mean molecular weight and isentropic exponent as shown in Table 1. Helium jets are an excellent analog for steam eruptions [*Kieffer and Sturtevant*, 1984]. Our numerical simulations are for nitrogen jets in order to benchmark and extend the laboratory experiments and examine the various timescales involved in shock formation and dissipation with internally consistent conditions. Therefore in order to extrapolate the experimental conclusions to Mount St. Helens, we consider which properties are independent, or weakly dependent, on gas properties such as the isentropic exponent γ (Mach disk standoff distance, characteristic times), and which are dependent on γ (Mach disk diameter) [*Ashkenas and Sherman*, 1966].

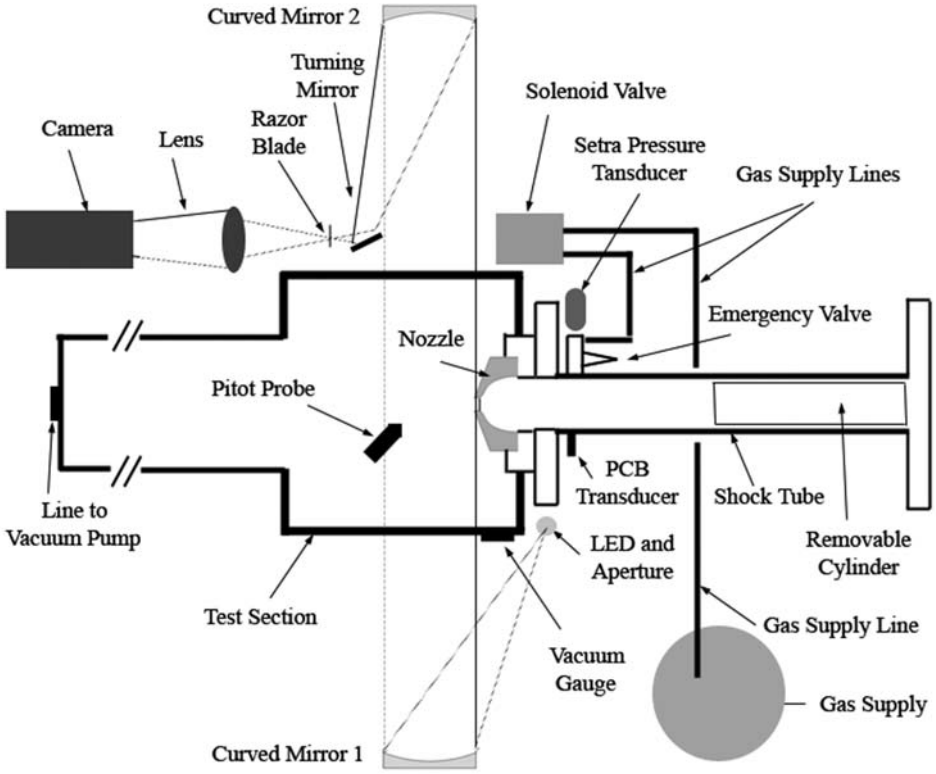

Figure 2. Schematic of experimental setup (not to scale). A diaphragm initially separating the high pressure reservoir from lower pressure surroundings is located at the nozzle throat. The reservoir length is adjusted by a series of removable cylinders of different lengths. The test gas fills the reservoir from the gas supply through the solenoid valve that is remotely controlled. Downstream from the diaphragm, the test section can be evacuated to 0.1 kPa and is optically transparent. The pitot probe triggers data acquisition for both the schlieren system and the pressure transducers in the reservoir. The schlieren setup is used to obtain images of the jet during reservoir discharge while the transducers record the initial burst pressure (Setra transducer) and the pressure profile (PCB transducer).

[19] Second, the geometry of the experiments is different from that at Mount St. Helens. In contrast to our unconfined laboratory jets, the blast at Mount St. Helens was confined on the bottom by terrain. During the directed blast, the blast fluid was free to expand three dimensionally out toward the north and around the mountain to the east and west. In the laboratory, experimental design requires a back plate for stability and this back plate influences the expansion near the vent, in particular by reducing the expansion to angles well below the Prandtl-Meyer angle. The blast fluid was constrained by a boundary at the ground, whereas in the lab experiments to date there is no simulated ground or topography. These experiments without geometric complications, however, are necessary for understanding the unsteady jet structures and are reference cases for more complex future experiments in progress.

2.1. Laboratory Experiments

[20] Experiments were conducted in an open-ended shock tube facility. A reservoir containing test gas initially pressurized up to 4.5 MPa exhausts either into the ambient atmosphere or into a vacuum capable test section (Figure 2). The reservoir is a constant 55 mm diameter pipe in which cylindrical blockages can be inserted to change the reservoir length in stages from 38 mm to 965 mm and vary the volume while maintaining similar one-dimensional internal gasdynamics. Mounted to the discharging end of the reservoir is one of two convergent nozzles with throat diameters, D, of 10 mm or 4 mm. A Mylar diaphragm is initially located at the nozzle throat, separating the high pressure reservoir from the downstream test region. The experiment initiates when the pressure difference across the diaphragm exceeds the yield strength of the Mylar and the diaphragm ruptures.

[21] Pressure ratios up to 250:1 are achieved by combining the reservoir with a vacuum capable test section evacuated down to 10 kPa minimum pressure (Figure 2). The Plexiglas test section is transparent for optical access and large enough to act as an unconfined volume for the initial diffracting shock and to ensure a negligible back pressure increase during the experiment. The test section pipe extension allows the turbulent downstream jet wake to propagate without interference and increases the total volume. A static pressure transducer (Setra 206) with a 5 ms response time measures the initial reservoir pressure. Dynamic pressure transducers (PCB 113A26) with 1 μs response times measure the pressure history in the reservoir during the jet exhaust.

[22] Data acquisition is triggered with the arrival of the initial shock wave at a sting-mounted dynamic pressure gauge (PCB 113A26) located in the free field, off axis from

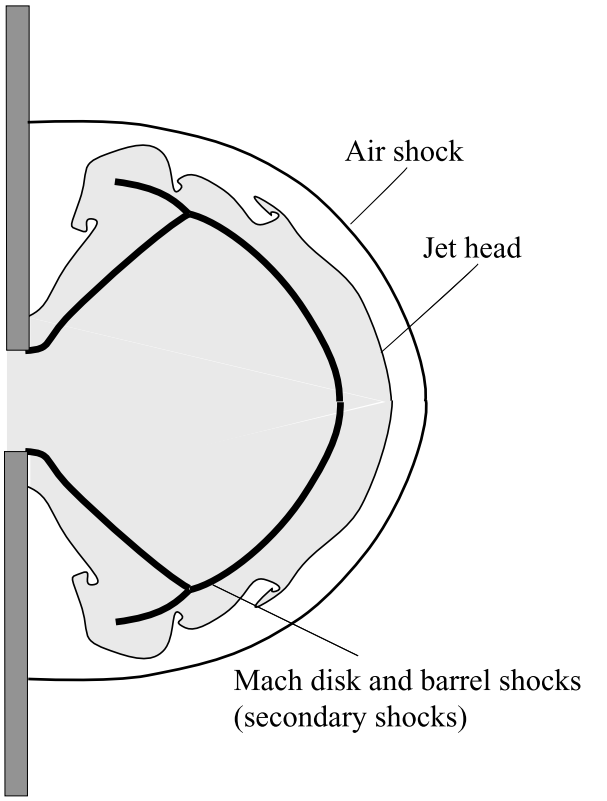

Figure 3. Schematic of flow features during the transient startup of a supersonic jet [after *Radulescu and Law*, 2007]. A secondary shock system consisting of barrel shocks and a Mach disk shock is formed in the jet head.

the jet exhaust. Single-shot schlieren images of the jet structure at selected times are obtained for each experiment. Light from a continuous white light LED point source is collimated to a field of view measuring 102 mm in front of the nozzle exit. The density gradients within the exhausting jet refract the light and yield gray scale schlieren images, recorded by a pco.1600 CCD camera (Cooke Corporation) with 100 μs exposure time at delays from 0 to 100 ms after diaphragm rupture preset using a Quantum Composer delay generator. Data acquisition with a single time origin allows schlieren images to be compared with the reservoir pressure history to yield the instantaneous pressure ratio for each image.

[23] Visualization of the discharging jet structure from each initial condition is constructed from a sequence of successive single-shot experiments. Five test conditions were selected, presented in Table 1. For each condition, experiments were run with four reservoir lengths L: 38 mm, 152 mm, 228 mm, and 965 mm, with resulting reservoir volume to nozzle area V_r/A_n ratios of 1.0, 8.5, 10, and 26 mm respectively for the 10 mm nozzle exit diameter.

2.2. Numerical Experiments

[24] The initial stages of jet formation are investigated with numerical simulations. The nonreacting Euler equations are solved with the Amrita environment developed by Quirk (http://www.amrita-cfd.org/doc, 1998a; http://www.amrita-cfd.org/doc, 1998b). An operator split scheme with HLLE flux and kappa-MUSCL reconstruction, incorporating an adaptive mesh refinement algorithm, was used. The Amrita framework has been demonstrated by *Quirk and Karni* [1997], *Hornung* [2002], and *Sharpe and Quirk* [2008] among others. Using Mount St. Helens as an example of a finite magma dome eruption, axisymmetric simulations are carried out for an equivalent reservoir with length 1300 m and diameter 328 m, corresponding to the hydraulic diameter of the 850 × 100 m vent proposed by *Donnadieu and Merle* [2001]. Selected simulations were also performed for length-to-vent diameter ratios corresponding to the experiments.

[25] The initial condition consists of a contact surface separating the high pressure reservoir and the ambient surroundings. As simulations are intended to augment the experimental results and focus on the processes of jet evolution and collapse for small reservoirs, the isentropic exponent was assumed to be constant and have a value of 1.4. As will be discussed in section 5, we justify using a constant specific heat ratio in the simulations from the observation that the Mach disk shock location does not depend on this parameter [e.g., see *Ashkenas and Sherman*, 1966]. Extrapolation boundary conditions were applied to simulate an unconfined volume into which the jet exhausts. The reservoir centerline is assumed to be an axis of symmetry. Simulations reproduced the laboratory situation of the vent as an orifice in a flat back plate. The reservoir end wall boundary condition is specified as reflective or extrapolative to examine both a finite or infinite volume respectively. We note that the simulations are used to examine the unsteady, gas dynamic wave interactions during jet evolution, and recognize limitations due to cylindrical symmetry and lack of viscous dissipation.

3. Laboratory and Numerical Results

[26] Upon sudden rupture of an overpressurized reservoir, an air blast wave precedes a jet head into the surrounding environment (Figure 3). The initial air shock and the jet head both propagate outwards and diffract due to the area

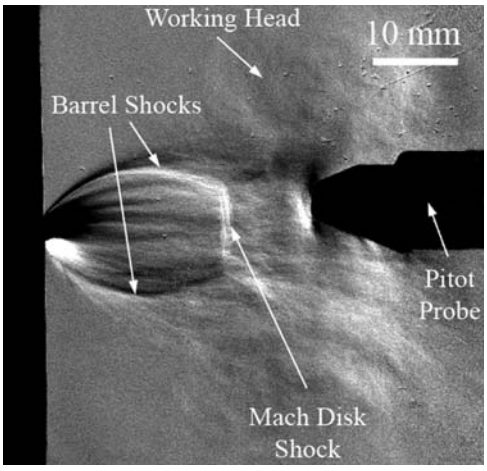

Figure 4. Schlieren image of jet structure during exhaust from a reservoir filled with nitrogen at initial pressure ratio of 150:1. Flow is from left to right. The image is triggered by the pitot probe located in the far right of the image.

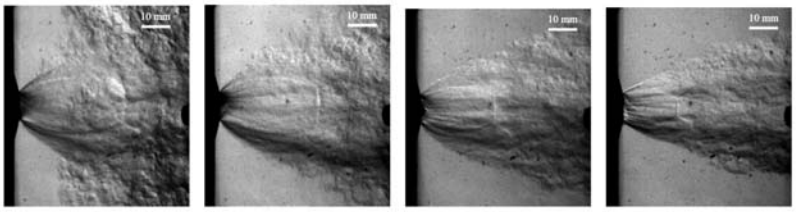

Figure 5. Schlieren images of the helium jet structure exhausting from a 96.5 cm long reservoir into ambient air. Flow is from left to right. The reservoir was filled with helium at initial pressure ratio of 41:1, with subsequent instantaneous pressure ratios of (a) 40:1, (b) 35:1, (c) 23:1, and (d) 14:1. Note the first possible image at 0.2 ms is not shown because the turbulent mixing of the jet head restricts imaging of the Mach disk and barrel shocks. Image acquisition is triggered by the arrival of the blast wave at a pressure gauge, evident as the small black object on the right side of each frame, and times are shown relative to the diaphragm burst.

change. A secondary shock system consisting of barrel and Mach disk shocks forms in the jet head within a few vent diameters, and then propagates downstream. The transient startup of the jet structure and normal Mach disk shock have been examined in detail [e.g., *Radulescu and Law*, 2007], assuming that flow at the vent is steady for the time of formation, as in the case of an infinite reservoir. In this work, we examine how these processes are affected by a finite reservoir.

3.1. Experimental Images of Jet Structure

[27] Because of experimental constraints in triggering the camera, our first images are taken ~0.2 ms after rupture of the diaphragm (Figure 4). The characteristic features of an early stage underexpanded jet are evident by this time. The jet expands outward from the nozzle exit, forming symmetrical barrel shocks laterally, a shear layer outside of the barrel shocks, and a normal Mach disk shock. The air shock and much of the starting vortex, also called the "working head", are out of the images to the right with some turbulent mass still visible on the right side of the photos.

[28] Similar underexpanded jet structures are observed in each image. The jet reaches a steady state location when the Mach disk and barrel shocks are fully formed. However, in the finite reservoir case, as the initial pressure ratio is decreased, the Mach disk shock location moves closer to the vent exit. Downstream from the Mach disk shock, there is a region of reacceleration that can form a secondary cell, resulting in a "shock diamond" pattern [*Love*, 1958].

[29] Temporal histories of the jets as the reservoir pressures decrease, called the "blowdown", were constructed from single-shot schlieren images acquired at selected times after diaphragm rupture (Figures 5 and 6). The first image is obtained at the time of incident blast wave arrival at the pitot probe. In all experiments we see the Mach disk shock fully developed at its equilibrium location by the time the camera is triggered, and we use the numerical simulations to investigate processes prior to this time (section 3.2). As the reservoir pressure decreases as a function of time, the Mach disk shock propagates back toward the vent and decreases in diameter (Figures 5b–5d and 6b–6e). The barrel shocks contract into the flow and the overall area of the supersonic region decreases through the blowdown. At a pressure ratio ~5:1, there is a transition from Mach reflection to regular reflection, and a series of oblique shock waves appear in the exhaust; the Mach disk disappears altogether as the reservoir

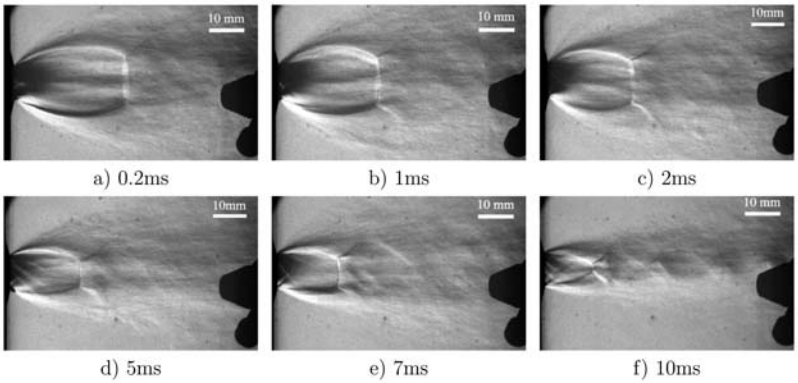

Figure 6. Schlieren images of a nitrogen jet exhausting from a 38 mm long reservoir into ambient air. Flow is from left to right. The reservoir was filled with nitrogen at initial pressure ratio of (a) 40:1, with subsequent instantaneous pressure ratios of (b) 28:1, (c) 17:1, (d) 13:1, (e) 8:1, and (f)6:1. Image acquisition is triggered by the arrival of the blast wave at a pressure gauge, evident on the right side of each frame as the black object, and times shown are relative to diaphragm burst.

pressure decreases past this threshold (Figure 6f). As the reservoir pressure continues to decrease beyond that shown in Figures 5d and 6f, the nozzle throat unchokes and the flow is everywhere subsonic until finally ambient equilibrium conditions are reached and the reservoir is empty.

[30] Reservoir pressures for each image were obtained by measurement of the time history of pressure within the reservoir. The pressure history is determined by the initial reservoir volume, the nozzle exit area, the speed of sound of the gas, c_0, and the ratio R_p of instantaneous reservoir pressure $P_r(t)$ to the initial reservoir pressure $P_r(0)$. From *Kieffer and Sturtevant* [1984] the reservoir pressure ratio R_p as a function of time is

$$R_p(t) = \frac{P_r(t)}{P_r(0)} = \left(\frac{tc_0}{V_r/A_n} \left[\left(\frac{\gamma - 1}{2} \right) \left(\frac{2}{\gamma + 1} \right)^{\frac{\gamma+1}{2(\gamma-1)}} \right] + 1 \right)^{\frac{2\gamma}{1-\gamma}}. \quad (1)$$

[31] Experimental nondimensional plots for pressure and time rate of change of pressure are compared to equation (1) (Figure 7). In nondimensional coordinates, the experimental pressure histories collapse on to a single curve (equation (1) and Figure 7a).

[32] Hysteresis has been reported in the literature for the location of the Mach disk shock [*Irie et al.*, 2003] as discussed in section 1. In order to justify comparing our conclusions about hysteresis, we present the the nondimensional time derivative for the pressure ratio decay (Figure 7b). The nondimensional time rate of change of the pressure discharge at the initial stages of blowdown is comparable to that found by *Irie et al.* [2003] who report hysteresis.

[33] In a steady state underexpanded jet, the Mach disk shock location normalized by the exit diameter is linearly dependent on the square root of the reservoir-to-ambient pressure ratio for pressures greater than 15:1 [*Ashkenas and Sherman*, 1966] (Figure 8). A power law empirical fit for pressure ratios between 15:1 and 10000:1 was derived from continuous flow facility experimental data by [*Ashkenas and Sherman*, 1966]

$$x_m/D = 0.67(P_r/P_a)^{0.5}, \quad (2)$$

where P_a is the ambient pressure. The method of characteristics [*Love*, 1958], or an approximate solution [*Adamson and Nicholls*, 1959], can be used to calculate the location of the shear layer which is assumed to act as a flow boundary as a theoretical justification of equation (2). As in a nozzle expansion, the Mach disk shock location can be predicted assuming the pressure increase across the shock is required to match ambient conditions.

[34] If the vent pressure changes as a function of time, the exhausting jet structure is affected. For example, in a spherical blast with continuously decreasing postshock pressure, experiments [*Boyer*, 1960], and analysis [*Friedman*, 1961] show the secondary shock structure initially propagates outwards, but then recedes back toward the origin. In a numerical study of open-ended shock tubes by *Haselbacher et al.* [2007], oscillatory transient behavior was observed and shear layer instability was suggested as one mechanism that might send disturbances upstream into the subsonic region. A similar phenomenon was observed in numerical simulations of *Ogden et al.* [2008].

[35] From our experimental data (Figures 5 and 6) we measured the location of Mach disk shock relative to the vent at selected times after diaphragm rupture. Reservoir pressures at these times are known from the measurements in the reservoir. The normalized Mach disk shock locations are shown in Figures 9 and 10 for nitrogen and helium jets respectively. The difference in initial burst pressures creates no observable difference in Mach disk shock location as a function of pressure ratio. For each initial burst pressure, the distance falls initially on the empirical curve at the correlating maximum pressure, then propagates along this curve as the pressure ratio between the reservoir and downstream conditions decreases.

[36] The Mach disk locations for pressure ratios above 15:1 for both nitrogen and helium fall along a log linear plot, regardless of the isentropic exponent. The slight scatter to the data in this region is within experimental error. Mach disk shock location agrees with locations given by the Ashkensas-Sherman relation (equation (2)), and is independent of the isentropic exponent.

3.2. Numerical Simulations of Jet Start-Up and Blowdown

[37] In order to clarify the flow history prior to the first images obtained experimentally, we carry out axisymmetric simulations. We examine the jet structure during startup and estimate timescales required for the formation and evolution of a Mach disk shock. As described in section 2.2, an infinite reservoir with extrapolated boundary conditions applied at the left boundary of the domain is first considered. Simulated schlieren images are shown in Figure 11.

[38] Upon opening of the vent, the initially stationary fluid in the reservoir accelerates to choked conditions at the exit plane of the nozzle as predicted by one-dimensional shock tube theory [*Liepmann and Roshko*, 2001]. An unsteady expansion fan is generated at the corner. The head of the expansion fan propagates along the air blast wave, causing the shock to diffract (Figure 11a). A steady Prandtl-Meyer expansion fan exists at the corner. The pressure and velocity decrease through the expansion fan is greater than the decrease behind the diffracting blast wave [*Friedman*, 1961]. As a result, a secondary shock system is formed, initially offset from the vent exit in the corner region of the steady expansion [*Skews*, 1967a; *Schultz*, 2000; *Radulescu and Law*, 2007]. The centerline flow is one-dimensional and unaffected by these processes until the arrival of the unsteady expansion fan. The secondary shock system is the origin of the first Mach disk and barrel shocks in an underexpanded jet. As the unsteady expansion fan propagates toward the centerline, the secondary shock system extends. The Mach disk and barrel shock system propagate toward the vent centerline (Figure 11b), and within a few vent diameters the Mach disk shock reaches the centerline (Figure 11c). The flow continues to evolve with the Mach disk shock propagating downstream behind the initial blast (Figures 11d–11h).

[39] In Figure 11h, the Mach disk shock has reached its steady state location, although the structure is not yet steady. As previously observed by *Haselbacher et al.* [2007] and *Lacerda* [1987], the Mach disk shock initially overshoots its

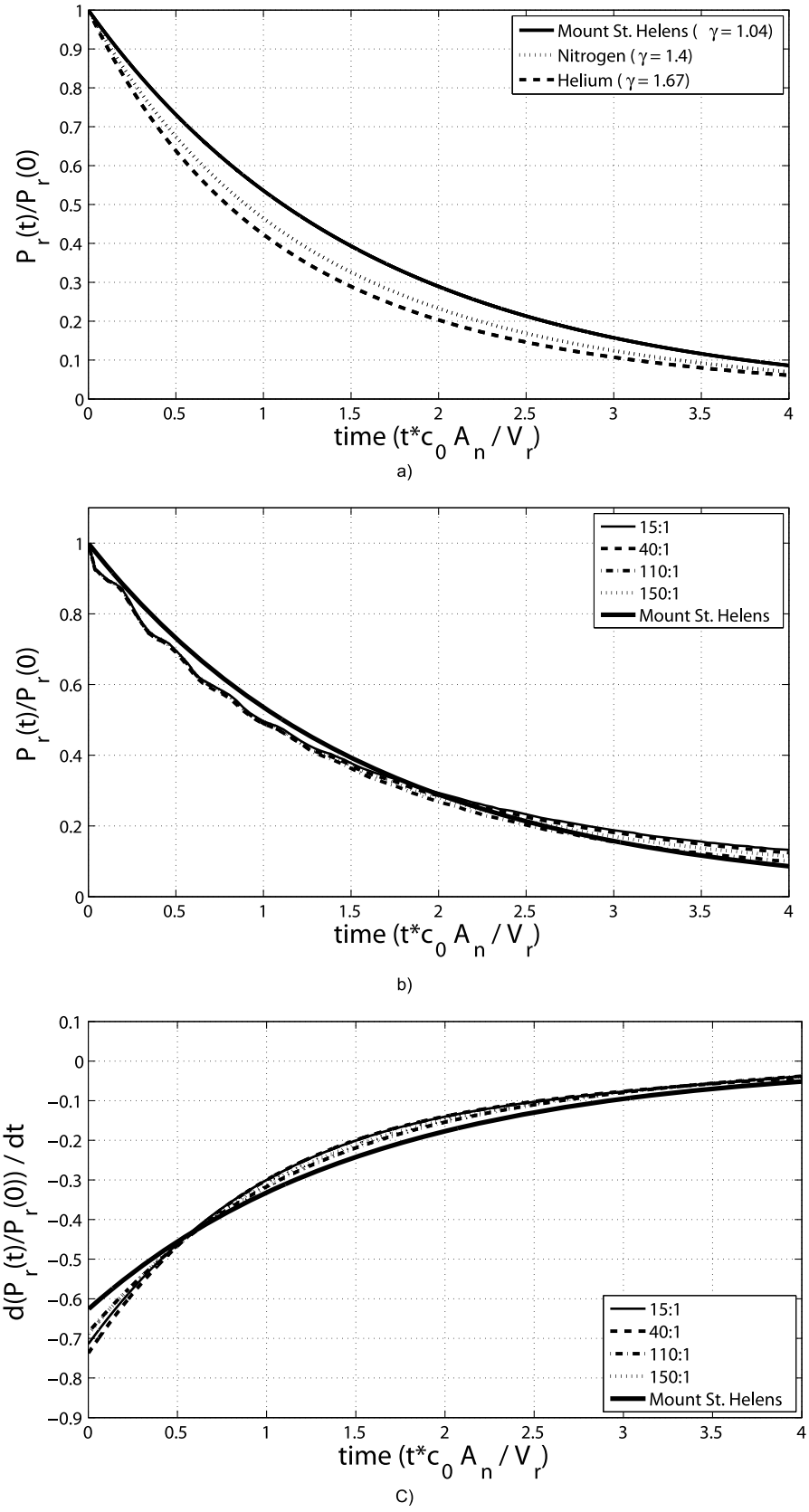

Figure 7. Nondimensionalized (a) pressure versus time from equation (1) for γ = 1.04, 1.4, and 1.67; (b) pressure versus time for experimental conditions with initial pressure ratios of 150:1, 100:1, 40:1, and 15:1; and (c) time rate of change of pressure versus time for experimental conditions described in Figure 7b).

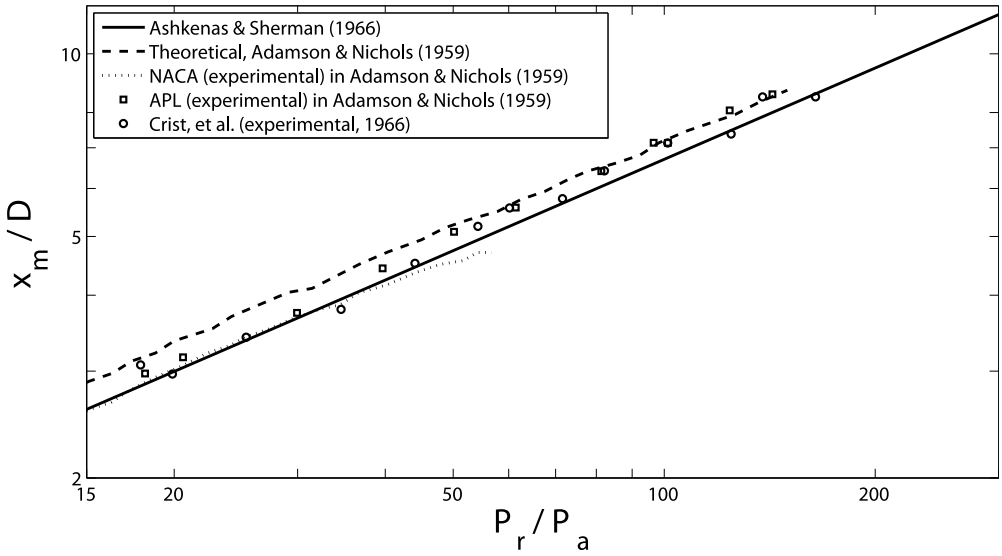

Figure 8. Normalized Mach disk shock location, x_m/D, versus reservoir to ambient pressure ratio, P_r/P_a. Data and theory are for a steady state underexpanded jet.

equilibrium location and then exhibits damped oscillation about the steady state value. For a heavy jet (SF_6) into nitrogen, the overshoot is about 20%, or a Mach disk shock location of 8.4 km for a vent diameter of 850 m. *Lacerda* [1987] reports the nondimensional Mach disk arrival time is similar for heavy and light jets.

[40] To examine the earlier phases of eruption from a finite chamber, simulations were carried out with a reflective boundary condition applied at the end wall of the reservoir (Figure 12). The external flow field of the finite reservoir case is identical to the infinite reservoir case during the formation of the secondary shock system (Figures 12a–12c); the Mach disk shock reaches the vent centerline at the same time in both the finite and infinite reservoir simulations. After rupture of the vent, an expansion wave propagates back into the reservoir (Figures 12a–12c). In the finite reservoir case, this wave reflects and propagates back toward the vent, decreasing the reservoir pressure (Figure 12d). The

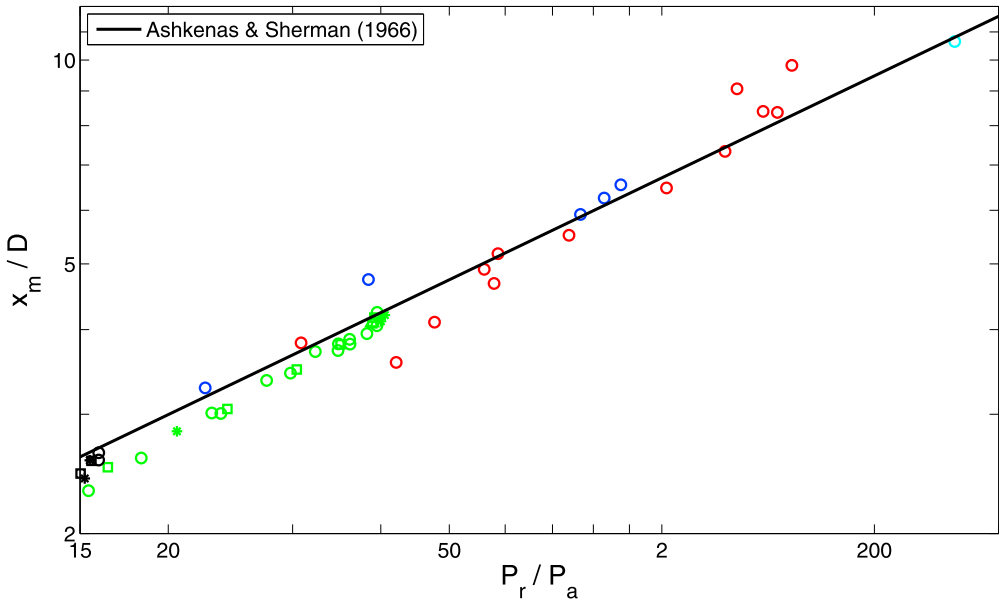

Figure 9. Mach disk shock location, x_m/D, versus reservoir to ambient pressure ratio, P_r/P_a for unsteady nitrogen jets. Initial reservoir-to-ambient pressure ratios were 250:1 (cyan), 150:1 (red), 100:1 (blue), 40:1 (green), and 15:1 (black). The symbols, asterisk, square, circle, and triangle, correspond to reservoir lengths of 96.5 cm, 22.8 cm, 15.2 cm, and 3.8 cm, respectively.

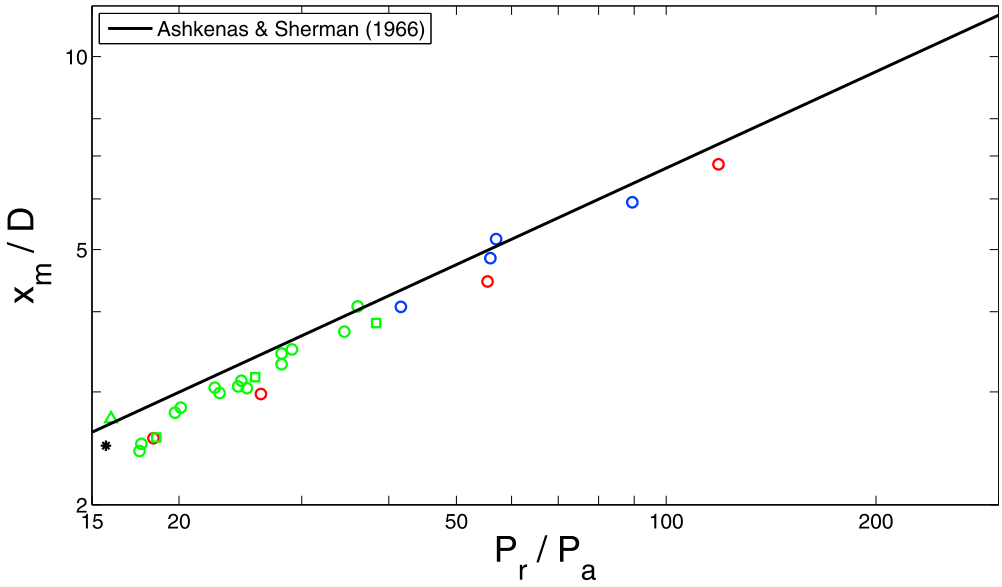

Figure 10. Mach disk shock location, x_m/D, versus reservoir to ambient pressure ratio, P_r/P_a for finite reservoir helium jets. Initial reservoir-to-ambient pressure ratios of 150:1 (red), 100:1 (blue), 40:1 (green), and 15:1 (black). The symbols, asterisk, square, circle, and triangle, correspond to reservoir lengths of 96.5 cm, 22.8 cm, 15.2 cm, and 3.8 cm, respectively.

reflected expansion strongly diffracts upon reaching the area change and is only just evident in the images as it propagates toward the Mach disk shock. In Figure 12d, the expansion head is approximately three-quarters of way to the Mach disk shock. The expansion wave interacts with the Mach disk shock, however the shock continues to propagate for some distance (Figure 12f). The simulations show the Mach disk shock reaches a maximum distance that is 86% of the equilibrium location for this reservoir dimension.

[41] The collapse of the jet structure as the reservoir is depleted is first evident near the vent as the expansion angle decreases and the shear layers move inward (Figures 12f and 12g). The Mach disk shock begins to propagate back toward the vent (Figures 12g and 12h). This is consistent with the model of *Adamson and Nicholls* [1959] in which the shear layers act as the boundary of the expanding flow and the Mach disk shock location is determined by extent of the expansion. A key result from the simulations is that the jet

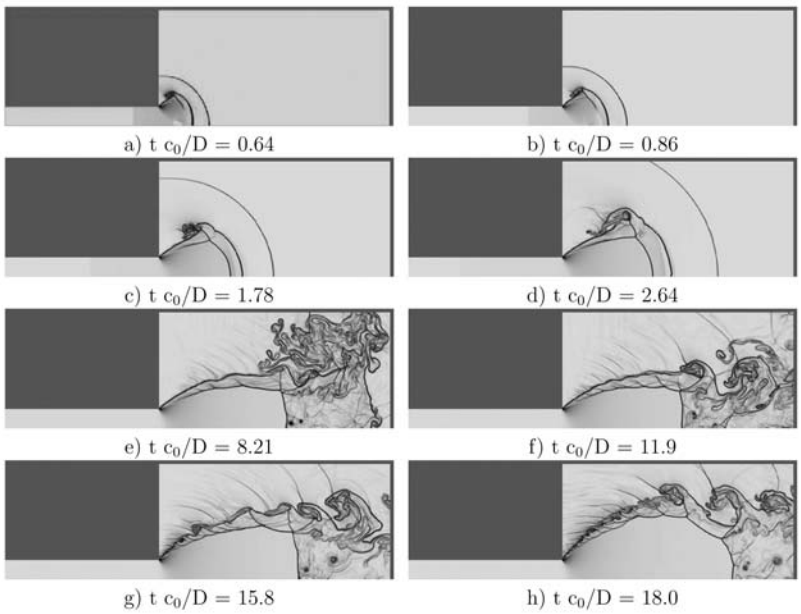

Figure 11. Evolution of an nitrogen jet from an infinite reservoir with 328 m diameter vent, with initial pressure ratio of 40. The calculation is axisymmetric about the reservoir centerline. The equilibrium Mach disk shock location for this pressure ratio is 8.2 times the vent radius.

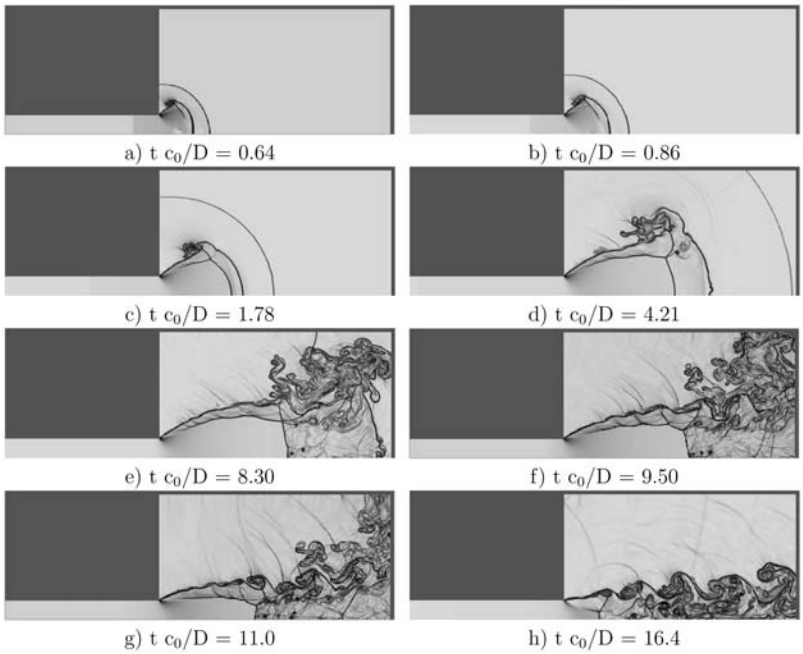

Figure 12. Evolution of an nitrogen jet from a finite reservoir with 1300 m depth with 328 m diameter vent, with initial pressure ratio of 40. The calculation is axisymmetric about the reservoir centerline.

structure begins to collapse at a time at which the vent approaches a subsonic, or unchoked, condition, as discussed in more detail in section 4.2.

4. Discussion

[42] The results presented in section 3 indicate there is no difference in the location of the Mach disk shock for finite versus infinite reservior jets. However, there must be a limiting case when the reservoir becomes so small no shocks can form other than the initial atmospheric shock. Therefore we discuss the results in the context of Mount St. Helens and vulcanian eruptions and present timescales relevant to jet features that will help to quantify the finite reservoir effects.

[43] We have developed the ideas above in the context of the vent conditions for vulcanian eruptions and extended them to the directed blast at Mount St. Helens because so much is known about plausible initial conditions for this event. The criteria that we have developed can be applied more generally, and we hope that this discussion will stimulate new observations on the mass ejected and duration of the cannon-like vulcanian eruptions.

[44] Supersonic conditions are indicated in the 1975 Ngauruhoe eruptions by a variety of phenomena: the documentation of an atmospheric shock traveling at Mach 1.8; a high speed flow front following closely behind the shock at a velocity of 300–600 m/s; and inferred reservoir pressures on the order of hundreds of bars [*Woods*, 1995; *Morrissey and Chouet*, 1997]. As mentioned in the introduction, we assume that each vulcanian eruption ejected roughly 0.5×10^6 m^3 of ejecta over a time of about 10 seconds. At Soufrière Hills, bursts lasting 10 to 20 seconds arose from a conduit of 30 m diameter and the order of 1000 m length [*Druitt et al.*, 2002; *Clarke et al.*, 2002a] The volume ejected averaged 3.0×10^5 m^3. We take these as the typical dimensions of vulcanian systems. For Mount St. Helens, we assume a reservoir containing 0.1 km^3 of material erupted through a vent that is 850 × 100 × 1300 m dimension [*Donnadieu and Merle*, 2001].

4.1. Equilibrium Mach Disk Shock Location

[45] The fact that our results for the finite reservoir jet show the same trend for pressure ratios above 15:1 as those in equation (2) indicates that we can use the underexpanded jet model for explosive volcanic jets. The standoff distances produced by the Ashkenas and Sherman data fit (equation (2)), for Mach disk shock in typical vulcanian eruptions are a few hundred meters. For example, at a pressure ratio of 150:1, it would be located 240 m from the vent exit. For Mount St. Helens, assuming a pressure ratio of 150:1 and a characteristic vent dimension of 850 m, the Mach disk shock location is predicted from the Ashkenas and Sherman empirical fit to be on the order of 7 km from the vent. For pressure ratios of 100:1 and 250:1, these distances are 5.7 km and 9 km respectively.

[46] *Kieffer* [1981, 1982, 1984] postulated the Mach disk shock at Mount St. Helens to be further out at ~11 km. Part of the difference between this result and our prediction of between 5.7 km and 9 km arises because she used a vent diameter of 1 km in contrast to the 850 m used in this paper. For that geometry, the correct downstream distance according to equation (2) would be 8.2 km. The remaining difference arises from two other causes: Kieffer mistakenly used a pressure ratio of 230:1 in this one calculation instead of 150:1 used for the rest of the model in those papers, a mistake only discovered during the course of the current work. This would have placed the shock at 10 km. Secondly, the coefficient obtained from *Joint Army, Navy, NASA, Air Force* [1975] was 10% larger than given by equation (2). This raised the distance she calculated to 11 km (for a

Table 2. Duration of Supersonic Flow at the Vent and the Formation Time of the Mach Disk Shock for the Systems Considered in This Study[a]

System	$\frac{P_r(0)}{P_a}$	t_{de}	t_{MDS}
Laboratory nitrogen jet	150	19 ms	36 μs
Laboratory nitrogen jet	40	12 ms	36 μs
Laboratory helium jet	150	7 ms	–
Laboratory helium jet	40	4 ms	–
vulcanian	100	65 s	~1 s
vulcanian (steam)	100	7 s	–
Mount St. Helens	100	84 s	12 s
Mount St. Helens	150	93 s	12 s
Mount St. Helens	250	104 s	12 s

[a]Here t_{de} is the duration of supersonic flow at the vent and t_{MDS} is the formation time of the Mach disk shock. Data for laboratory reservoirs with V_r/A_n = 1.0 mm are shown.

pressure ratio of 150:1), in contrast to the corrected distance of 6–9 km reported here (for pressure ratios of 100:1 to 250:1).

4.2. Process of Formation of the Mach Disk Shock and Timescales of the Start-Up and Blowdown

[47] We examine criteria for establishment of the supersonic jet features in the flow as well as their duration and distances from the vent. The start-up and blowdown processes are characterized by four different timescales: the duration of supersonic flow at the nozzle exit, t_{de}; the formation time of the Mach disk shock, t_{MDS}; the travel time required for the Mach disk shock to reach its final equilibrium position, t_{eq}; and the time at which the Mach disk shock begins to significantly collapse away from its equilibrium position back toward the vent, t_{coll}. If the time required to form the Mach disk shock is greater than the duration of supersonic flow at the nozzle, the Mach disk shock never forms at its final equilibrium position. If the travel time required for the Mach disk shock to reach its final equilibrium position is greater than the time at which the jet begins to collapse and move it back toward the vent, the shock never forms. We now examine these four timescales.

4.2.1. Duration of Supersonic Flow at the Vent, t_{de}

[48] Supersonic flow is maintained at the vent until the reservoir pressure ratio decreases to

$$\frac{P_r(t)}{P_a} = R_p \frac{P_r(0)}{P_a} = \left(\frac{\gamma+1}{2}\right)^{\frac{\gamma}{\gamma-1}}, \tag{3}$$

where $P_r(t)$ is the instantaneous reservoir pressure, P_a is the ambient pressure, and $P_r(0)$ is the initial reservoir pressure. For the nitrogen isentropic exponent γ = 1.4, the critical pressure ratio is $\frac{P_r}{P_a}$ is 1.89:1; for helium, γ = 1.67, it is 2.05:1; and for the pseudogas with γ = 1.04, the critical pressure ratio is 1.67:1. The blowdown time to reach this critical pressure ratio t_{de} depends on V_r/A_n through equation (1) as

$$\frac{c_0 t_{de}}{V_r/A_n} = \left[\left(\frac{\gamma+1}{2}\right)^{-0.5}\left(\frac{P_a}{P_r(0)}\right)^{\frac{1-\gamma}{2\gamma}} - 1\right] \times \left(\frac{2}{\gamma-1}\right)\left(\frac{2}{\gamma+1}\right)^{-(\gamma+1)/2(\gamma-1)}. \tag{4}$$

For the open shock tube model, V_r/A_n is L, the length of the conduit. For a short, wide reservoir with a small exit conduit, V_r/A_n is significantly larger than the physical depth of the conduit. From equation (1), we calculate the nondimensional and dimensional times, $\frac{t_{de}c_0A_n}{V_r}$ and t_{de}, for the duration of supersonic flow at the vent for the laboratory, vulcanian, and Mount St. Helens eruptions (Table 2).

[49] For a 150:1 initial pressure ratio and the laboratory conditions of V_r/A_n = 1 mm and V_r/A_n = 26 mm, t_{de} is 19 ms and 495 ms respectively. For a typical vulcanian eruption with V_r/A_n = 1000 m and γ = 1.04, we conclude that the duration of supersonic flow at the vent is 65 s. For a water-dominated vulcanian eruption plume the analog helium would have a shorter flow duration: 7 s. For Mount St. Helens at a pressures of 100:1, 150:1, and 250:1, t_{de}, is 84, 93, and 104 s respectively. These times will next be compared to estimates of the times required for Mach disk shock formation.

4.2.2. Formation Time of the Mach Disk Shock, t_{MDS}

[50] An initial estimate of formation time of the secondary shock system that produces the Mach disk shock, t_{MDS}, may be obtained by a geometric consideration of the time to arrival of the first unsteady expansion characteristic. This leads to diffraction of the initial shock, at the centerline (Figure 13). An analogous flow field occurs when a shock wave propagating in a duct encounters an abrupt area change and undergoes a multidimensional diffraction.

[51] We perform a geometric analysis analysis based on Skews' formulation of the propagation of a corner signal in postshock flow [*Skews*, 1967b, 1967a]. In time, t, the incident (unaffected) wave has traveled a distance of $U_f t$ where U_f is the wavefront velocity. The head of the unsteady expansion (corner signal) propagates at the sound speed of the gas exiting the vent, c, with the particle velocity, u. These two vectors form the angle, α, shown in Figure 13. The distance the corner signal propagates may be compared to the vent radius $D/2$ to obtain an expression for the lead wave arrival time at the centerline t

$$\tan\alpha = \frac{D/2}{U_f t} = \frac{\sqrt{c^2 - (U_f - u)^2}}{U_f} \tag{5}$$

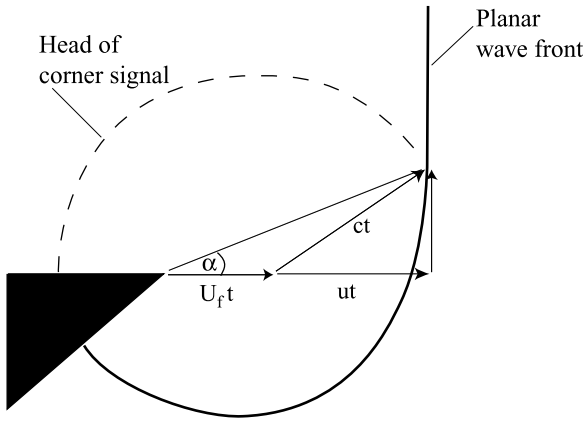

Figure 13. Schematic showing Skew's construction for corner signal propagation in postshock flow [*Skews*, 1967b].

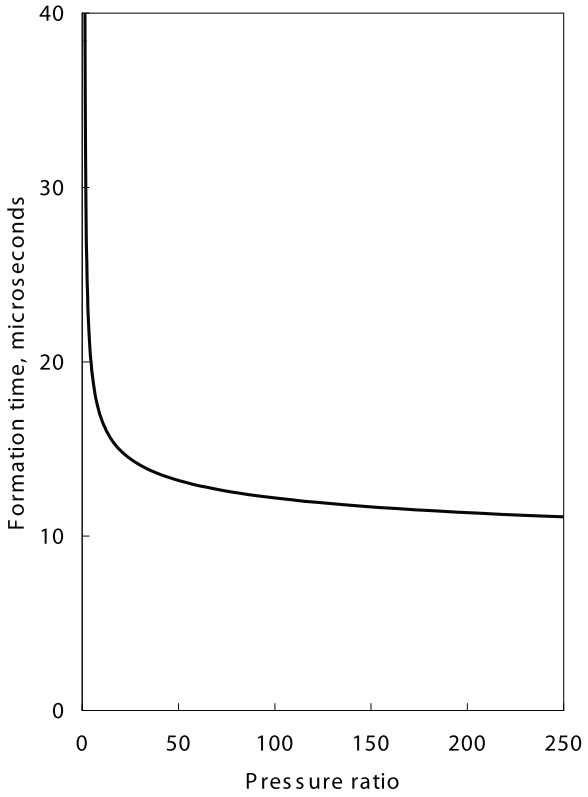

Figure 14. Calculated formation times based on Skews' formulation for unsteady expansion head arrival at the vent centerline for nitrogen jets exhausting from 10 mm diameter vent.

$$t = \frac{D}{2\sqrt{c^2 - \left(U_f - u\right)^2}}. \tag{6}$$

For the experimental nitrogen jets, we assume the incident shock Mach number can be predicted from the pressure ratio assuming unsteady one-dimensional shock tube gasdynamics [*Liepmann and Roshko*, 2001]. The sound speed and flow velocity are calculated at the postshock state. The formation time is then a function of the gas composition, the vent diameter, and the pressure ratio, or alternatively the incident shock Mach number. Calculated values of formation time as a function of pressure ratio are shown in Figure 14. The present experimental work examines initial pressure ratios from 15:1 to 250:1. For a nitrogen discharge from a 10 mm vent in the present experiments, the initial estimate for appearance of a secondary shock system varies from 16 to 11 μs for these pressures respectively. The formation time is longest for the smallest pressure ratios, decreasing steeply as the pressure ratio increases until becoming relatively insensitive to pressure at ratios greater than about 50:1.

[52] To obtain an initial estimate of the secondary shock formation time for volcanic jets, we assume that near the vent, the leading air shock and the jet head are in close proximity such that the corner signal propagates through the dusty gas. (The dusty gas has a lower sound speed than air, so this assumption results in an overestimation of the time required for initial shock diffraction in air.) The dusty gas has a sound speed at the vent of 103 m/s and we assume the fluid velocity is close to the wavefront velocity. In this case, the formation time is $\sim \frac{D}{2c}$, the time for a corner signal to reach the centerline. An initial estimate for the time required for a Mach disk shock to be created on the centerline in a dusty gas jet head is therefore is estimated to be about 0.15 s for a typical vulcanian eruption, and about 4 s for Mount St. Helens based on a vent diameter of 850 m.

[53] However, the secondary shock does not extend to the unsteady expansion head, but propagates some distance behind [*Skews*, 1967b; *Radulescu and Law*, 2007], as shown by the simulations in Figures 11 and 12. The time required for a Mach disk shock to reach the vent centerline, t_{MDS}, will be underestimated by the above analysis. We therefore measure the time for the Mach disk shock to reach the centerline from the numerical simulations. For nitrogen jets with pressure ratios over the range 40:1 to 250:1, we find

$$\frac{c_0 t_{MDS}}{D} = 1.3. \tag{7}$$

No appreciable dependence of formation time on pressure ratio was observed over the range of pressure ratios considered in this study, consistent with the estimations based on Skews' formulation. The formation time was the same for both infinite and finite reservoirs as the Mach disk shock formed much earlier than the arrival time of the reflected expansion wave at the aspect ratios considered in this study.

[54] Thus for an open-ended shock tube with diameter 10 mm corresponding to the experimental nozzle diameter, this formation time is 36 μs. This time is a factor of three greater than obtained based on Skews' formulation. We assume a similar scaling applies to vulcanian systems and Mount St. Helens, and will use the order of magnitude t_{MDS} to be a less than a second for vulcanian eruptions and of the order of 12 seconds for Mount St. Helens. We note that the Mach disk shock forms before any significant pressure drop in the reservoir. These formation timescales are in good agreement with simulations by *Ogden et al.* [2008] when scaled to their dimensions. In conclusion, since $t_{MDS} < t_{de}$ for the vulcanian systems and for Mount St. Helens, we find there to be sufficient time for the Mach disk shock to form in the flow field in the vicinity of the vent.

4.2.3. Travel Time for the Mach Disk Shock to Reach Its Final Equilibrium Location, t_{eq}

[55] We next consider the propagation of the Mach disk shock toward its equilibrium or steady state location. We base our estimates of the travel time, t_{eq}, on two previous studies: the experimental work of *Lacerda* [1987], and the numerical simulations of *Ogden et al.* [2008]. *Lacerda* [1987] measured the outward propagation of jet head and the Mach disk shock for a heavy (SF_6) and matched (N_2) jets into nitrogen at a pressure ratio of 100 using high-speed shadowgraph movies. For this pressure ratio, the equilibrium Mach disk shock location is $x_m/D = 6.7$ (equation (2)). The jet head arrival time at this location is $\frac{tc_0}{D} = 5.6$, which is also consistent with one-dimensional shock tube calculations. The nitrogen jet velocity was measured to be similar to the heavy jet velocity. The Mach disk shock arrived at the steady state location at a nondimensional time of $\frac{t_{eq}c_0}{D} = 6.8$ for the heavy jet and 7.3 for the matched jet. The nondimensional time between jet head arrival and Mach disk

Table 3. Comparison of Propagation Timescales t_{eq} Based on Scaling the Experimental Results of *Lacerda* [1987] and the Numerical Results of *Ogden et al.* [2008], With Jet Collapse Timescales t_{coll} for the Systems of This Study[a]

System	$\frac{P_r(0)}{P_a}$	t_{eq},s	t_{coll},s
Laboratory nitrogen jet	100	0.15×10^{-3}	0.2
vulcanian	100	1	65
Mount St. Helens	100	54	84
Mount St. Helens	150	78	93
Mount St. Helens	250	80	104

[a]If $t_{eq} \leq t_{coll}$, we estimate a Mach disk shock has time to form at its equilibrium location.

shock arrival is thus approximately 1.2 and 1.7 for heavy and matched jets respectively. This result is not corrected out to x_m/D of 8.2 which would correspond to a pressure ratio of 250:1. A constant jet head velocity may be assumed, consistent with the measurements of *Lacerda* [1987] for $x/D <$ 8.4 and 6.4 for heavy and matched jets respectively, however the Mach disk shock is decelerating as it approaches the steady state location, so the above estimate for the delay between jet head and Mach disk shock arrival maybe a considered a minimum value.

[56] *Ogden et al.* [2008] conducted a series of time-dependent simulations of the pseudogas jets erupting from vents of varying diameter and overpressure ratio up to 100. From these simulations, the nondimensional time of jet head and Mach disk shock arrival at the steady state location is 2.6 and 3.8 respectively. While these travel times are a factor of two less than those of *Lacerda* [1987], the difference between jet head and Mach disk shock arrival times is also 1.2. We thus use the above studies to examine t_{eq} timescales for laboratory jets, vulcanian eruptions, and the directed blast of Mount St. Helens as

$$\frac{t_{eq}c_0}{D} = \frac{x_m c_0}{uD} + 1.2, \tag{8}$$

where $\frac{x_m c_0}{Du}$ represents the nondimensional time of jet head arrival at the equilibrium location x_m/D. The jet head velocity u is calculated from one-dimensional shock tube theory and assumed to be assumed to be constant while the jet propagates, as measured in the experiments of *Lacerda* [1987]. The nondimensional time between the jet head and Mach disk shock arrival at the equilibrium location is 1.2 for a matched jet, as discussed above.

[57] For our nitrogen and helium laboratory jets at pressure ratios of 250:1, the Mach disk shock is established at its equilibrium location within the time required to take the first image (~0.2 ms). Assuming a constant jet head velocity of 654 and 3500 m/s for nitrogen and helium jets, the jet head travel times are 0.1 and 0.02 m/s respectively. Experimental observations are thus consistent with the calculated Mach disk shock arrival time of 0.15 ms for the slower case of the nitrogen jet.

[58] For typical vulcanian eruptions, we assume a minimum jet head velocity approaching 400 m/s [*Nairn*, 1976], and calculate the the Mach disk shock arrives at its steady state in 1 s. For the vent diameter and local vent sound speed of Mount St. Helens, the Mach disk shock reaches 7 km downstream approximately 10 s after the jet head [*Lacerda*, 1987]. For a dusty gas reservoir initially at a pressure ratio of 150:1, the velocity at the vent is 103 m/s from *Kieffer* [1982, p. 386], reduced from the reservoir sound speed of 105 m/s. This would mean that it took 68 s for the jet head to reach the 7 km location of the Mach disk shock. Assuming that the Mach disk shock arrived 10 s after the jet head, this yields an estimate of 78 s for establishment of the Mach disk shock at its final location for Mount St. Helens. However, the reported average velocity of the directed blast over the direct blast zone was 130 m/s, with local variations in the velocity due to interactions with the topography [*Voight*, 1982]. In this case, the estimated establishment time would be at t_{eq} = 63 s + 10 s = 73 s.

4.2.4. Duration of the Mach Disk Shock Near the Steady State Location, t_{coll}

[59] In order to address the question of whether there is sufficient time for the Mach disk shock to reach the steady state location before the reservoir is depleted, we consider the process of shutdown of the jet and estimate the time at which it begins to occur, t_{coll}. As the jet forms, the shear layers define a diverging nozzle which contains the Mach disk and barrel shock system. Numerical simulations, described in section 3.2, show that as the jet collapses, the shear layer nozzle moves toward the vent. The Mach disk shock begins to retreat back toward the vent at a time that is comparable to the time at which the vent becomes subsonic, or unchoked. We can therefore estimate the collapse time to be approximately equal to the duration of supersonic flow at the vent

$$t_{coll} \approx t_{de}. \tag{9}$$

For vulcanian eruptions, t_{de} is 65 seconds, based on the discussion in section 4.2.1. For Mount St. Helens, t_{de}, is 84, 93, 104 seconds for initial reservoir pressure ratios of 100:1, 150:1, and 250:1 respectively.

[60] We compare these collapse times, t_{coll}, to the time required for the Mach disk shock to reach the equilibrium location, t_{eq}. For the vulcanian eruptions with pressure ratios of 100:1, t_{eq} (1 s) is substantially less than t_{coll} (65 s), indicating a Mach disk shock has time to form and propagate to the equilibrium location of x_m/D = 6.7 predicted by the steady state empirical fit [*Ashkenas and Sherman*, 1966]. For Mount St. Helens, at a pressure ratio of 150:1, t_{eq} is 1.2–1.5 times smaller than t_{de}, indicating that the Mach disk shock would have propagated a distance comparable to the steady state prediction of 7 km. Table 3 shows the timescale comparisons for the supersonic jets considered in this work.

[61] Taking $t_{coll} \leq t_{de}$, and evaluating equation (1) at the pressure ratio corresponding to an unchoked vent, given by equation (3), we obtain an expression for the minimum reservoir dimensions for Mach disk shock to exist at its equilibrium location at a given initial pressure ratio as

$$\frac{V_r/A_n}{D} \geq \frac{t_{eq}\left(\frac{\gamma-1}{2}\right)\left(\frac{2}{\gamma+1}\right)^{\frac{\gamma+1}{2(\gamma-1)}}}{\left[\left(\frac{\gamma+1}{2}\right)^{\frac{\gamma}{\gamma-1}}\frac{P_a}{P_r(0)}\right]^{\frac{1-\gamma}{2\gamma}} - 1}, \tag{10}$$

where t_{eq} is the travel time of the Mach disk shock to its nondimensional equilibrium position, given by equation (8). For an open-ended duct, $\frac{V_r/A_n}{D} = \frac{L}{D}$. Calculated values of

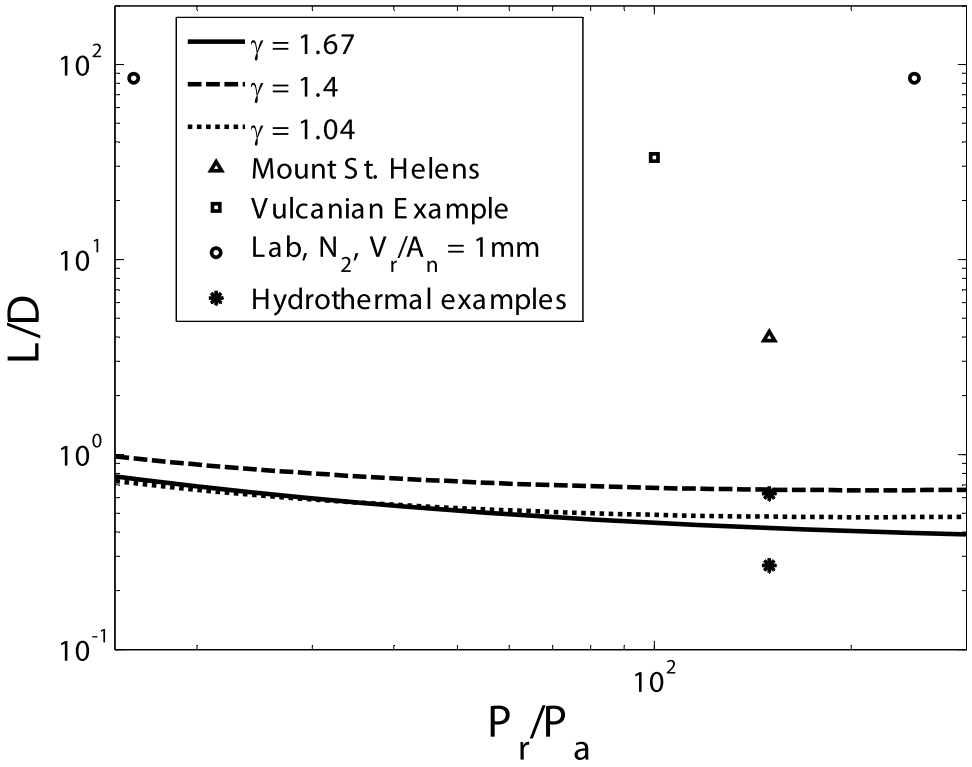

Figure 15. Calculated minimum reservoir dimensions for the formation of a Mach disk shock at its equilibrium location as a function of pressure ratio and isentropic exponent. vulcanian, Mount St. Helens, and laboratory examples shown for comparison. Laboratory experiments shown for an initial pressure ratio of 250:1. A discussion of the hydrothermal eruptions is found in section 4.

minimum $\frac{V_r/A_n}{D}$ as a function of pressure ratio and isentropic exponent are shown in Figure 15. The minimum reservoir dimensions are not strongly dependent on the isentropic exponent and are only weakly dependent on pressure ratio above 50:1. The minimum reservoir dimension is approximately one for large pressure ratios. In all cases considered, there is time for the Mach disk shock to be established at a distance comparable to the equilibrium location, before the collapse of the jet structure.

[62] What types of eruptions might preclude establishment of steady supersonic conditions? According to Figure 15, steady supersonic conditions would be precluded if L/D falls below the curve for the appropriate value of γ. We suggest that hydrothermal, phreatic, and phreatomagmatic eruptions are candidates because diameters, D, are plausibly large compared to the length of the conduit. As a possible example, consider the hydrothermal explosion craters in the Kawerau geothermal area of New Zealand [*Nairn and Wiradiradja*, 1980]. A large explosion about 14,000 years B.P. ejected 2×10^7 m^3 of rock. A crater of ~700 m in diameter was formed. There appear to be three 0.3 km to 0.5 km diameter craters. If we assume an extreme geometry, namely that the conduit diameter was equal to the crater diameter, we consider diameters of 300 m to 700 m. The conduit length might be equated to the inferred depth of explosive disruption, 190 m. For these extreme cases, we calculate an L/D is respectively 0.63 and 0.27, which would preclude steady supersonic conditions (Figure 15). Because the conduit diameter is likely to be significantly smaller, [see *Nairn and Wiradiradja*, 1980, Figure 4] establishment of steady supersonic flow is more likely even for these hydrothermal craters.

5. Conclusions

[63] In the introduction, we asked the following questions for the eruption of a supersonic jet from a finite reservoir: Does the flow history play a role in jet evolution? Can the jet structure be predicted from steady state theory if the reservoir pressure history is known? What is the timescale for establishment of supersonic flow fields and how does it compare with the reservoir discharge time? What are conditions under which a Mach disk shock is or is not established at its equilibrium position? We addressed these questions in the context of laboratory jets, hydrothermal eruptions, and vulcanian eruptions, and the Mount St Helens directed blast as examples of explosive eruptions from finite reservoirs.

[64] The Mach disk standoff distance for unsteady jets was measured from experimental images to follow the steady state Ashkenas and Sherman relation (equation (2)), for pressure ratios above 15:1 [*Ashkenas and Sherman*, 1966]. We found no evidence that flow history plays a role in jet evolution after the jet is established, in spite of pressure decay rates at the beginning of the blowdown that are comparable to *Gribben et al.* [2000], *Irie et al.* [2003], and *Welsh* [1997] who did report hysteresis. We compare and contrast the results of M. M. Orescanin and J. M. Austin

(Exhaust of underexpanded jets from finite reservoirs, submitted to Journal of Propulsion and Power). The standoff distance is independent of γ to within the resolution of the experiments in helium and nitrogen jets. The Mach disk is initially formed a few jet diameters downstream of the vent, then follows the jet head as it propagates downstream toward the steady state location.

[65] We identified four critical timescales for the establishment of the supersonic jet structure: the duration of supersonic flow at the nozzle exit, t_{de}; the formation time of the Mach disk shock, t_{MDS}; the travel time required for the Mach disk shock to reach its equilibrium position, t_{eq}; and the time at which the Mach disk shock begins significantly to collapse away from its equilibrium position, t_{coll}. Two critical timescale comparisons for the establishment of supersonic flow were identified. If $t_{MDS} \leq t_{de}$, the Mach disk shock has time to form on the vent centerline before the velocity at the vent becomes subsonic. If $t_{eq} \leq t_{coll}$, the Mach disk shock has time to propagate to its steady state location before the jet begins to collapse.

[66] From both theoretical analysis of diffracting shock waves and from axisymmetric numerical simulations, we estimated the timescales for formation of a Mach disk shock in the vicinity of the vent. At pressure ratios above 50:1, the near-field formation time of the Mach disk shock is independent of the pressure ratio. The timescales for jet establishment for conditions of the vulcanian and Mount St. Helens directed blast are on the order of one second to ten seconds, respectively. With plausible initial conditions for vulcanian eruptions, the duration of supersonic flow t_{de} at the nozzle throat is 65 s. For Mount St. Helens, t_{de} ranges from 84 to 104 seconds for pressure ratios of 100:1 and 250:1 respectively. In both these eruptions, therefore, these calculations indicate that the Mach disk shock had ample time to form.

[67] From simulations and experiments, we estimated the travel time of the Mach disk shock to the equilibrium position to be about 1 s for typical vulcanian eruptions consisting of mostly steam at a 100:1 pressure ratio and 78 s seconds for the Mount St Helens directed blast. In laboratory experiments, the Mach disk shock is established consistent with the analysis of t_{MDS}. Simulations show the evolving jet structure begins to collapse back toward the vent after a time comparable to t_{de}, when the flow at the vent approaches sonic conditions. Since the vent duration t_{de} and Mach disk establishment times are comparable, we concluded that for the systems considered in this study, the Mach disk shock can form and propagate a distance comparable to the equilibrium location.

[68] We used this approach to estimate the minimum reservoir dimensions required for the supersonic jet to be established as a function of the isentropic exponent and the pressure ratio. The minimum reservoir dimensions are not a strong function of γ, and so are similar for nitrogen, helium, and dusty gas jets. At large pressure ratios for an open duct, the minimum length over diameter ratio is approximately one. The minimum dimensions become approximately independent of pressure ratio above 50:1. We concluded that with the exception of extraordinarily large conduit diameters that might occur during hydrothermal, phreatic, and phreatomagmatic eruptions, equilibrium flow structures are formed in supersonic plumes in most eruptions.

[69] In summary, using a shock tube facility and numerical models we investigated unsteady eruption dynamics of supersonic jets up to pressure ratios of 250:1, higher than previously attained for such studies. We defined two timescales for the start-up process and two timescales for the termination process. Comparison between the startup and termination processes allows determination of the extent of unsteady flow. We concluded that for typical vulcanian eruptions and for the Mount St. Helens directed blast, steady conditions were obtained.

[70] The shock tube experiments should be of value to both the fluid dynamics and volcanology communities because, to our knowledge, such experimental data have not been previously available. In particular, they should be used as benchmarks for the numerous high pressure simulations of explosive volcanic eruptions. Even if the supersonic flow region is restricted to a few vent diameters, failure to capture the supersonic flow region accurately will lead to inaccuracies in the downstream subsonic flow region. We hope that these results will motivate new and innovative measurements of reservoir dimensions.

[71] **Acknowledgments.** NSF grant EAR06-09712, NSF grant SK2008-0035 8 ANTC and Charles R. Walgreen Jr. endowed funds to Susan W. Kieffer. We are grateful to James Quirk for the use of his code Amrita. We thank David Buchta at UIUC for performing modeling runs with a different code to cross-check our results.

References

Adamson, T. C., and J. A. Nicholls (1959), On the structure of jets from highly underexpanded nozzles into still air, *J. Aeronaut. Sci.*, *26*(1), 16–24.

Ashkenas, H., and F. S. Sherman (1966), Experimental methods in rarefied gas dynamics, *Tech. Rep. 32-869*, NASA, Washington, D. C.

Belousov, A., B. Voight, and M. Belousova (2007), Directed blasts and blast-generated pyroclastic density currents: A comparison of the Bezymianny 1956, Mount St. Helens 1980, and Soufrière Hills, Montserrat 1997 eruptions and deposits, *Bull. Volcanol.*, *69*(7), 701–740.

Boyer, D. W. (1960), An experimental study of the explosion generated by a pressurized sphere, *J. Fluid Mech.*, *9*, 401–429.

Brodsky, E. E., H. Kanamori, and B. Sturtevant (1999), A seismically constrained mass discharge rate for the initiation of the May 18, 1980 Mount St. Helens eruption, *J. Geophys. Res.*, *104*, 29,387–29,400.

Chojnicki, K., A. B. Clarke, and J. C. Phillips (2006), A shock-tube investigation of the dynamics of gas-particle mixtures: Implications for explosive volcanic eruptions, *Geophys. Res. Lett.*, *33*, L15309, doi:10.1029/2006GL026414.

Clarke, A. B., A. Neri, B. Voight, G. Macedonia, and T. H. Druitt (2002a), Computational modeling of the transient dynamics of the August 1997 vulcanian explosions at Soufrière Hills Volcano, Montserrat: Infuence of initial conduit conditions on near-vent pyroclastic dispersal, *Geol. Soc. London Mem.*, *21*, 319–348.

Clarke, A. B., B. Voight, A. Neri, and G. Macedonio (2002b), Transient dynamics of vulcanian explosions and column collapse, *Nature*, *415*, 897–901.

Donnadieu, F., and O. Merle (2001), Geometrical constraints of the 1980 Mount St. Helens intrusion from analogue models, *Geophys. Res. Lett.*, *28*, 639–642.

Druitt, T. H., et al. (2002), Episodes of cyclic Vulcanian explosive activity with fountain collapse at Soufrière Hills Volcano, Montserrat, *Geol. Soc. London Mem.*, *21*, 281–306.

Friedman, M. P. (1961), A simplified analysis of spherical and cylindrical blast waves, *J. Fluid Mech.*, *11*, 1–15.

Gribben, B. J., K. J. Badcock, and B. E. Richards (2000), Numerical study of shock-reflection hysteresis in an underexpanded jet, *AIAA J.*, *38*(2), 275–283.

Haselbacher, A., S. Balachandar, and S. W. Kieffer (2007), Open-ended shock tube flows: Influence of pressure ratio and diaphragm position, *AIAA J.*, *45*(8), 1917–1929.

Hornung, H. G. (2002), Hypersonic flow over bodies in tandem, *Shock Waves*, *11*(6), 441–445.

Irie, T., T. Yasunobu, H. Kashimura, and T. Setoguchi (2003), Characteristics of a Mach disk in the underexpanded jet in which the back pressure continuously changes with time, *J. Therm. Sci.*, *12*(2), 132–137.

Joint Army, Navy, NASA, Air Force (1975), Joint Army, Navy, NASA, Air Force Handbook of rocket exhaust plume technology, *Chem. Propul. Inf. Agency Publ. 263*, 237 pp., Columbia, Md.

Kieffer, S. W. (1981), Blast dynamics at Mount St. Helens on 18 May 1980, *Nature*, *291*, 568–570.

Kieffer, S. W. (1982), Fluid dynamics of the May 18 blast at Mount St. Helens, *U.S. Geol. Surv. Prof. Pap., 1250*, 379–400.

Kieffer, S. W. (1984), Factors governing the structure of volcanic jets, in *Explosive Volcanism: Inception, Evolution, and Hazards*, pp. 143–157, Natl. Acad., Washington, D. C.

Kieffer, S. W., and B. Sturtevant (1984), Laboratory studies of volcanic jets, *J. Geophys. Res.*, *89*(B10), 8253–8268.

Lacerda, N. L. (1987), On the start up of supersonic underexpanded jets, Ph.D. thesis, Grad. Aeronaut. Lab., Calif. Inst. of Technol., Pasadena, Calif.

Liepmann, H. W., and A. Roshko (2001), *Elements of Gasdynamics*, Dover, Mineola, N. Y.

Love, E. S. (1958), An approximation of the boundary of a supersonic axisymmetric jet exhausting into a supersonic stream, *J. Aeronaut. Sci.*, *25* (2), 130–131.

Melnick, O., and R. S. J. Sparks (2002), Dynamics of magma ascent and lava extrusion at Soufrière Hills Volcano, Montserrat, *Geol. Soc. London Mem.*, *21*, 539–555.

Morrissey, M. M., and B. A. Chouet (1997), Burst conditions of explosive volcanic eruptions recorded on microbarographs, *Science*, *275*, 1290–1294.

Nairn, I. A. (1976), Atmospheric shock waves and condensation clouds from Ngauruhoe explosive eruptions, *Nature*, *259*, 190–192.

Narin, I. A., and S. Self (1978), Explosive eruptions and pyroclastic avalanches from Ngauruhoe in February 1975, *J. Volcanol. Geotherm. Res.*, *3*, 39–60.

Nairn, I. A., and S. Wiradiradja (1980), Late Quaternary hydrothermal explosion breccias at Kawerau Geothermal Field, New Zealand, *Bull. Volcanol.*, *43*, 1–13.

Ogden, D. E., K. H. Wohletz, D. A. Glatzmaier, and E. E. Brodsky (2008), Numerical simulations of volcanic jets: Importance of vent overpressure, *J. Geophys. Res.*, *113*, B02204, doi:10.1029/2007JB005133.

Orescanin, M. M., and J. M. Austin (2010), Exhaust of underexpanded jets from finite reservoirs, *J. Propul. Power*, in press.

Quirk, J. J., and S. Karni (1997), On the dynamics of shock-bubble interaction, *J. Fluid Mech.*, *318*, 129–163.

Radulescu, M. I., and C. K. Law (2007), The transient start of supersonic jets, *J. Fluid Mech.*, *578*, 331–369.

Reed, J. W. (1987), Air pressure waves from Mount St. Helens eruptions, *J. Geophys. Res.*, *92*, 11,979–11,992.

Saito, T., T. Kitmura, K. Takayama, N. Fujii, and H. Taniguchi (1995), Numerical simulation of blast waves propagation induced by eruption of volcanoes, in *19th International Symposium on Shock Waves, Marseille, France, July 26–30, 1994*, edited by L. Z. Dumitrescu, pp. 385–390, Springer, Berlin.

Schultz, E. (2000), Detonation diffraction through an abrupt area expansion, Ph.D. thesis, Grad. Aeronaut. Lab., Calif. Inst. of Technol., Pasadena, Calif.

Sharpe, G. J., and J. J. Quirk (2008), Nonlinear cellular dynamics of the idealized detonation model: Regular cells, *Combust. Theory Modell.*, *12*, 1–21.

Skews, B. W. (1967a), The perturbed region behind a diffracting shock wave, *J. Fluid Mech.*, *29*, 705–719.

Skews, B. W. (1967b), The shape of a diffracting shock wave, *J. Fluid Mech.*, *29*, 297–304.

Sparks, R. S. J., J. Barclay, E. S. Calder, R. A. Herd, J.-C. Komorowski, R. Luckett, G. E. Norton, L. J. Ritchie, B. Voight, and A. W. Woods (2002), Generation of a debris avalanche and iolent pyroclastic density current on 26 December (Boxing Day) at Soufrière Hills Volcano, Montserrat, *Geol. Soc. London Mem.*, *21*, 409–434.

Takayama, K., and T. Saito (2004), Shock wave/geophysical and medical applications, *Annu. Rev. Fluid Mech.*, *36*, 347–379.

Valentine, G. A. (1994), Multifield governing equations for magma dynamics, *Geophys. Astrophys. Fluid Dyn.*, *78*, 193–210.

Valentine, G. A. (1998), Eruption column physics, in *From Magma to Tephra: Modeling Physical Processes of Explosive Volcanic Eruptions*, edited by A. Freundt and M. Rosi, pp. 91–138, Elsevier, New York.

Valentine, G. A., and K. H. Wohletz (1989), Numerical models of Plinian eruption columns and pyroclastic flows, *J. Geophys. Res.*, *94*, 1867–1887.

Voight, B. (1982), Timescale for the first moments of the May 18 eruption, *U.S. Geol. Surv. Prof. Pap., 1250*, 69–92.

Welsh, F. P. (1997), Shock reflection hysteresis in low density underexpanded jets, *Tech. Rep. DRA TR DRA/DWS/WX9/CR97361*, Def. Eval. and Res. Agency, Farmborough, U. K.

Woods, A. W. (1995), A model of Vulcanian explosions, *Nucl. Eng. Design*, *155*, 345–357.

J. M. Austin, Department of Aerospace Engineering, University of Illinois at Urbana-Champaign, 306 Talbot Laboratory, MC-236, 104 S. Wright St., Urbana, IL 61801, USA. (jmaustin@illinois.edu)

S. W. Kieffer and M. M. Orescanin, Department of Geology, University of Illinois at Urbana-Champaign, 245 Natural History Building, 1301 W. Green St., Urbana, IL 61801, USA.